ISSN 1009 – 3095 *Journal of Zhejiang University SCIENCE* V.4, No.3, P.241 – 253, May – June, 2003
http://www.zju.edu.cn/jzus; http://www.periodicals.com.cn; jzus@zju.edu.cn

Raman crystal lasers in the visible and near-infrared

EICHLER H.J.[†1], GAD G.M.A.[1], KAMINSKII A.A.[2], RHEE H.[†1]

([1] *Optical Institute, Technical University of Berlin, Strasse des 17. Juni 135, D-10623 Berlin, Germany*)
([2] *Institute of Crystallography, Russian Academy of Sciences, Leninsky prospekt 59, 117333 Moscow, Russia*)

[†]E-mail: eichler@physik.tu_berlin.de; hanjo@physik.tu_berlin.de

Received Apr.1, 2003; revision accepted Apr.16, 2003

Abstract: Raman lasers based on potassium gadolinium tungstate and lead tungstate crystals pumped by $a \approx 120$ ps Nd: YAG laser at 1.064 μm were developed. High reflection mirrors for the Stokes wavelength have been used to generate near-infrared and eye safe spectral region of 1.15 – 1.32 μm. Second harmonic generation of the generated Raman lasers was observed. Eifficient multiple Stokes and anti-Stokes picosecond generation in 64 crystals have been shown to exhibit stimulated Raman scattering on about 700 lines covering the whole visible and near-infrared spectrum. All stimulated Raman scattering (SRS) wavelengths in the visible and near-infrared spectrum are identified and attributed to the SRS-active vibration modes of these crystals.

Key words: Raman laser, Crystals, Raman seattering, Nonlinear optics, Stokes
Document code: A **CLC number:** O437.3

INTRODUCTION

Frequency conversion processes in particular, stimulated Raman scattering (SRS) in crystals provide new coherent light sources and extend the number of emission wavelengths of currently available solid state lasers. Raman conversion system can be created by single pass stimulated Raman scattering and Raman laser with an external pumping or internal pumping optical system. The SRS efficiency can be quite high and further improvement is possible by arranging the Raman crystals between two mirrors in such a way that they form an optical resonator. Such Raman lasers convert up to 80% of the pump power into the first Stokes power. The created Raman laser lines cover the near and mid infrared, visible and near ultraviolet spectral regions. Applications exist in spectroscopy, e.g. detecting water vapour pollutants in the atmosphere by lidar techniques.

At present, the SRS-active media most commonly used in Raman lasers are the cubic $Ba(NO_3)_2$, monoclinic $KGd(WO_4)_2$ and tetragonal $PbWO_4$ crystals which have been investigated intensively during the last few years (Eremenko *et al.*, 1980; Andrjunas *et al.*, 1985; Karpukhin *et al.*, 1986; Berenberg *et al.*, 1987; Kaminskii *et al.*, 1998; 1999; He *et al.*, 1997; Zverev *et al.*, 1999). Among these crystals $PbWO_4$ has several advantages. It is very stable and unlike $Ba(NO_3)_2$ it does not require moisture protection. Due to the possibility to grow $PbWO_4$ in big sizes with high optical quality by the ordinary Czochralski pulling technique, costs are very low in contrast to α-$KGd(WO_4)_2$ crystals which can only be grown in big size by the very expensive top-seed flux method. The generation characteristics of a $Ba(NO_3)_2$ Raman laser with pumped by a narrowband tunable nanosecond Ti: Sapphire laser were studied (Orlovich *et al.*, 2000) Operation of all-solid-state compact pulsed Nd: $KGd(WO_4)_2$ Raman laser pumped by a cw laser diode was demonstrated (Grabtchikov *et al.*, 2000). Furthermore, passively Q-switched 1.35 μm diode pumped laser operation in neodymium-doped potassium gadolinium tungstate had been achieved (Grabtchikov *et al.*, 2001). Recently, laser action in linear and ring Raman oscillators based on $PbWO_4$ crystals in nanosecond region were demonstrated (Kaminskii *et al.*, 2000).

In this work, we present efficiently stimulated Raman scattering based on 64 crystals (see Table 1), where about 700 lines had been ob-

served. Furthermore, we demonstrate a new potential of the $KGd(WO_4)_2$ and $PbWO_4$ crystals (Kaminskii *et al*., 2000; Findeisen *et al*., 1999; Gad *et al*., 2003), namely the ability to generate highly efficient near-infrared and eye safe spectral region of 1.160 – 1.320 μm wavelength.

Table 1 List of investigated Raman-active crystals which are suitable for Raman lasers and their symmetry from dissertation of J. Findeisen, 1999 and dissertation of Gad, 2003 at the Technical University of Berlin

Crystal	Name	Symmetry	Size(mm)
α'-Al_2O_3	Corundum	Orthorhombic	11 × 8 × 6
α-$C_{14}H_{12}O$	α-4-Methylbenzo-phenone	Monoclinic	≈15
β'-BaB_2O_4	Barium Borate	Trigonal	3 × 4 × 13
β'-$Gd_2(MoO_4)_3$	Gadolinium Molybdate	Orthorhombic	12 × 11 × 9
$Ba(NO_3)_2$	Barium Nitrate	Cubic	10 × 10 × 60
$Ba_2NaNb_5O_{15}$	Barium Sodium Niobate		ø 4 × 30
$BaSr(NbO_3)_2$	Barium Strontium Niobate		ø 6 × 18
BiB_3O_6	Bismuth Triborate	Monoclinic	12 × 6 × 3
$Bi_4Ge_3O_{12}$	Bismuth Germanate	Cubic	50
$Bi_4Si_3O_{12}$	Bismuth Silicate	Cubic	50
$Ca_3Ga_2Ge_3O_{12}$	Calcium Gallium Garnet	Cubic	ø 5 × 22
$Ca_3Ga_2Ge_5O_{14}$	Calcium Gallium Germanate	Cubic	ø 5 × 26
$Ca_4Gd(BO_3)_3O$	Calcium Gadolinium Oxoborate	Monoclinic	30 × 5 × 6
$Ca(NbGa)_2Ga_3O_{12}$	Calcium Niobium Granate	Cubic	5 × 14 × 9
$Ca(NbO_3)_2$	Calcium Niobate	Cubic	ø 6 × 18
$Ca(NO_3)_2/KNO_3$ glass	Nitrate glass		4 × 10 × 15
$Ca_2Mg_2SiO_7$	Calcium Magnesium Silicate	Tetragonal	5 × 7 × 13
$CaWO_4$	Calcium Tungstate	Tetragonal	(J) 7 × 20
$Ca_2Zn_2SiO_7$	Calcium Zinc Silicate	Tetragonal	6 × 7 × 14
$CdWO_4$	Cadmium Tungstate	Monoclinic	20 × 16 × 10
$C_{15}H_{19}N_3O_2$(AANP)	2-Adamantylamino-5-Nitropyridine	Orthorhombic	
$C_{16}H_{15}N_3O_4$(MNBA)	4′-Nitrobenzylidene-3-Acetamino-4-Methoxyaniline	Monoclinc	12 × 15 × 1
$C_{13}H_{10}O$	Benzophenone	Orthorhombic	≈15
$[C(NH_2)_3]Zr[N(CH_2COO)_3]_2 \cdot H_2O$	GuZN-III	Orthorhombic	8
$CsNO_3$	Cesium Nitrate	Cubic	5 × 7 × 10
$Dy_2(MoO_4)_3$	Dysprosium Molybdate	Tetragonal	11 × 8 × 10
$Gd_3Ga_5O_{12}$	Gadolinium Gallium Garnet	Cubic	ø 5 × 21
$Gd_3Sc_2Ga_3O_{12}$	Gadolinium Scandium Gallium Garnet	Cubic	ø 5 × 23
$GdVO_4$	Gadolinium Vanadate	Tetragonal	
HJO_3	Hydrogen Iodate	Orthorhombic	20 × 22 × 16
$KAl(SO_4)_2 \cdot 12H_2O$	Alum	Cubic	20 × 20 × 20
$KDy(WO_4)_2$	Calcium Dysprosium Tungstate	Monoclinic	8 × 10 × 20
$KGd(WO_4)_2$	Potassium Gadolinium Tungstate	Monoclinic	18 × 12 × 9
KIO_3	Potassium Iodate	Triklin	4 × 5 × 11
$KLa(MoO_4)_2$	Potassium Lanthanum Molybdate	Tetragonal	13 × 6 × 9
$KLuWO_4$	Potassium Lutetium Tungstate		ø 5 × 16
$KTiOPO_4$	Potassium Titanyl Phosphate	Orthorhombic	5 × 5 × 15

Continued in the next page

Crystal	Name	Symmetry	Size(mm)
$KY(MoO_4)_2$	Potassium Yttrium Molybdate	Orthorhombic	10 × 11 × 8
$KY(WO_4)_2$	Potassium Yttrium Tungstate	Monoclinic	17 × 9 × 13
$LaBGeO_5$	Lanthanum Boron Germanate	Trigonal	14 × 8 × 10
LiB_3O_5	Lithium Borate	Orthorhombic	4 × 4 × 12
$LiCaAlF_6$	Lithium Calcium Aluminum Fluoride	Trigonal	35 × 10 × 8
$LiIO_3$	Lithium Iodate	Hexagonal	10 × 15 × 30
$LiNbGeO_5$	Lithium Niob Germanate	Orthorhombic	12 × 9 × 11
$LiNbO_3$	Lithium Niobate	Trigonal	9 × 9 × 8
$NaBrO_3$	Sodium Bromate	Cubic	2 × 6 × 14
NaCl	Sodium Chlorate	Cubic	34 × 6 × 18
$NaClO_3$	Sodium Chlorate	Cubic	50 × 23 × 10
$NaLa(MoO_4)_2$	Sodium Lanthanum Molybdate	Tetragonal	12 × 11 × 10
$(NaPO_3)_x$	Polyphosphate glass		ø 15 × 40
Na_2SO_4	Sodium Sulfate	Orthorhombic	3 × 6 × 15
$NaY(WO_4)_2$	Sodium Yttrium Tungstate	Tetragonal	8 × 12 × 16
$PbCl_2$	Lead Chloride	Orthorhombic	6 × 7 × 10
$PbMoO_4$	Lead Molybdate	Tetragonal	6 × 5 × 16
$PbWO_4$	Lead Tungstate	Tetragonal	10 × 10 × 100
$Sc_2(MoO_4)_3$	Scandium Molybdate	Orthorhombic	11 × 7 × 11
$Sr(NO_3)_2$	Strontium Nitrate	Cubic	4 × 7 × 16
$SrMoO_4$	Strontium Molybdate	Tetragonal	5 × 6 × 12
$SrWO_4$	Strontium Tungstate	Tetragonal	4 × 8 × 11
TeO_2	Tellurium Oxide	Orthorhombic	6 × 7 × 20
$Y_3Al_5O_{12}$(ceramic)	Yttrium Aluminum Garnet	Cubic	10 × 10 × 60
$Y_3Al_5O_{12}$(crystal)	Yttrium-Aluminum Garnet	Cubic	ø 6 × 19
YVO_4	Yttrium Vanadate	Tetragonal	
$ZnWO_4$	Zinc Tungstate	Monoclinic	10 × 20 × 8

PROPERTIES OF SELECTED ACTIVE CRYSTALS SUITABLE FOR RAMAN LASERS

Some properties of selected Raman active crystals are listed in Tables 1 and 2. At present, the most used materials in solid-state Raman lasers are cubic Barium-Nitrate $Ba(NO_3)_2$, monoclinic potassium Gadolinium tungstate KGd $(WO_4)_2$ and tetragonal lead tungstate $PbWO_4$ crystals.

In cubic $Ba(NO_3)_2$ the vibrational mode with energy of $\omega_R = 1047\ cm^{-1}$ can be used to create Raman lasers in the visible as well as IR region (He *et al.*, 1997; Findeisen *et al.*, 2000). Barium nitrate belongs to symmetry group T_h^6 and has a refractive index of $n \approx 1.6$. For the Raman laser experiments, crystals with lengths up to 60 mm were used in sealed housings for moisture protection with AR coating.

$KGd(WO_4)_2$ has two vibrational modes with strong interaction. With excitation in b-axis orientation (010) parallel to the pump beam propagation laser action at both $\lambda = 1159$ nm with phonon energy of $\omega_{R1} = 768\ cm^{-1}$ and $\lambda = 1177$ nm with phonon energy of $\omega_{R2} = 901\ cm^{-1}$ had been demonstrated in a crystal of 47 mm length (Findeisen *et al.*, 2000). The refractive index is $n \approx 2$ in this direction. The modified Czochralski method was used to grow monoclinic $KGd(WO_4)_2$ belonging to the symmetry group C_{2h}^6. The crystal structure was centrosymmetric, i.e. any $\chi^{(2)}$-activity was blocked by its inversion symmetry. Polished and uncoated $KGd(WO_4)_2$ crystals were used to develop several Raman lasers in the IR region (Findeisen *et*

al., 1999). This emission can be converted into the yellow region of interest in medical applications (removal of vascular lesions). $KGd(WO_4)_2$ can be doped with Nd leading to a self-stimulating Raman laser.

Tetragonal $PbWO_4$ crystal is very stable, cheap and can be grown in big sizes with high optical quality also by the modified Czochralski method. It belongs to the symmetry group C_{4h}^6. The structure of this crystal is centrosymmetric and without $\chi^{(2)}$-activity. The crystal was used to demonstrate Raman lasers in IR region that have been frequency doubled into yellow and red regions which generally is difficult to generate by other solid-state lasers. In these experiments, crystals with lengths of up to 70 mm with polishing and without coating were used. The refractive index was $n \approx 2.2$ for c-axis orientation of the samples used in these experiments (Findeisen *et al*., 1999).

The exhition of strong Raman scattering in $KGd(WO_4)_2$ and $PbWO_4$ crystals can be explained by, first their structural symmetry associated with totally symmetric vibrational modes of the molecular WO_4^- groups and second, the covalent bonds between the oxygen and tungstate atoms allowing a great change of polarizability.

Table 2 Properties of selected Raman-active crystals which are suitable for Raman lasers

Crystal	Optical transparency(μm)	Raman shift(cm^{-1})	Raman gain ($cm\ GW^{-1}$)	Raman Line width (cm^{-1})	Applications beside SRS
$Ba(NO_3)_2$	0.35 – 1.8	1047	10 – 11	0.42	Laser
BiB_3O_6	0.29 – 3.2	604	2.9	7 – 11	SHG, THG, laser
$KGd(WO_4)_2$	0.34 – 5.5	901	3.3	5.6	Laser
		768	4.4	6.6	
$PbWO_4$	0.33 – 5.5	901	3	4.2	Laser, γ-ray scintillators
		323		7.5	
$Y_3Al_5O_{12}$-ceramic		370	0.1 ± 0.05	5.7	Solid state lasers
YVO_4		890	4.5	3	Laser

STIMULATED RAMAN SCATTERING SETUP

For the excitation of single-pass SRS in Raman crystals, we use a picosecond Nd: YAG mode-locked laser with two-stage amplifiers. The master-oscillator generates a polarized pulse train with energy of about 2 mJ at wavelength of 1.064 μm. An external Pockels cell pulse slicer transmits only the central pulse with duration of $\approx$ 120 ps (FWHM) and energy of about 200 μJ. The following Nd: YAG amplifier increases the energy of this polarized single pulse up to 5 mJ. An optional external KD*P frequency doubler with 25% efficiency converts the pulse to wavelength 0.532 μm with a pulse duration of about 80 ps. The pump beam was focused into the oriented samples by a lens with focal length 150 – 250 mm, resulting in a beam waist diameter of about 75 – 100 μm. The spectral composition of the Stokes and anti-Stokes lines was investigated with a grating monochromator and Si-CCD sensor.

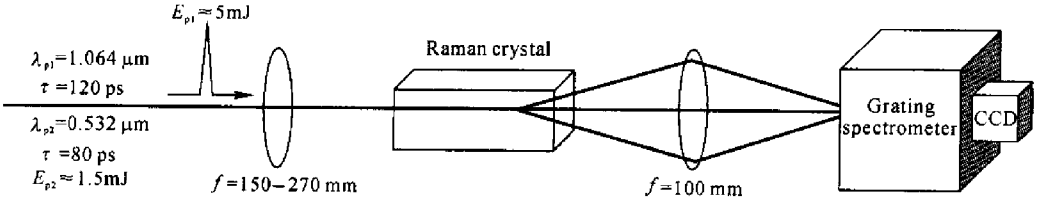

Fig.1 Experimental setup for single-pass SRS measurements in Raman crystals with excitation wavelengths at 1.064 μm and 0.532 μm

STIMULATED RAMAN SCATTERING RESULTS

1. Stimulated Raman spectra of $Ba(NO_3)_2$, $PbWO_4$ and $KGd(WO_4)_2$

Fig. 2a shows Stokes and anti-Stokes lines of a $Ba(NO_3)_2$ crystal. One Stokes and four anti-Stokes lines are connected with the SRS-active vibration mode $\omega_R = 1047\ cm^{-1}$. Due to the CCD-sensitivity drop-off (Fig. 2b), the intensity of the Stokes line is strongly reduced compared to the anti-Stokes lines so that only one Stokes line appears.

In $PbWO_4$ crystal Stokes and anti-Stokes lines were connected with the known SRS-active vibration mode $\omega_{R1} = 901\ cm^{-1}$ in addition to the previously unknown SRS-active mode at $\omega_{R2} = 323\ cm^{-1}$ (Fig. 3).

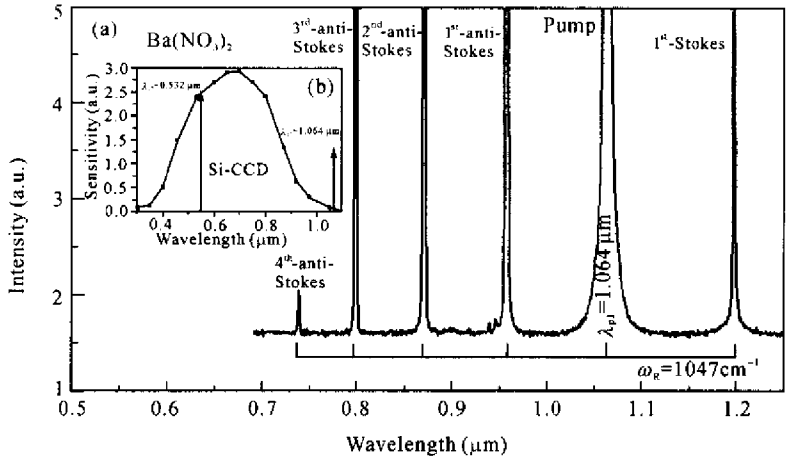

Fig. 2 (a) SRS single-pass spectra of $Ba(NO_3)_2$ crystal with excitation at 1064 nm; (b) Spectral sensitivity of the Si-CCD sensor

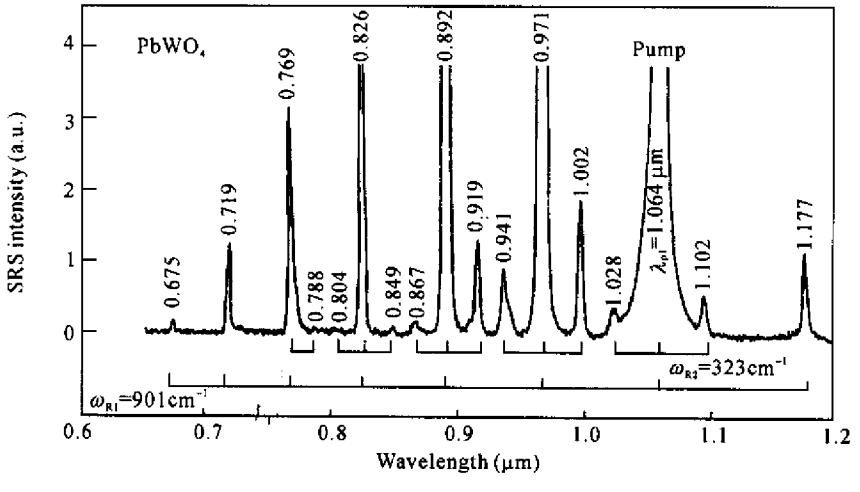

Fig. 3 SRS single-pass spectra of $PbWO_4$ crystal with excitation at 1064 nm

In Fig. 4a Stokes and anti-Stokes lines of a $KGd(WO_4)_2$ crystal are shown. The crystal was pumped with the foundamental frequency at $\lambda_{P1} = 1.064\ \mu m$ and its frequency doubled line at $\lambda_{P2} = 0.532\ \mu m$. The electric field vector of the pump beam is perpendicular to c axis of the crystal $E \perp c$. The spectra was obtained under b(aa)b excitation geometry. In this configuration only the vibrational mode with phonon energy of $\omega_{R1} = 901\ cm^{-1}$ was observed. Fig. 4b shows Stokes and anti-Stokes lines of a $KGd(WO_4)_2$ crystal. The crystal was pumped with the funda-

mental frequency at $\lambda_{P1} = 1.064$ μm and its frequency doubled line at $\lambda_{P2} = 0.532$ μm. The spectra was obtained under b(cc)b excitation geometry. In this case ($E \perp a$) only the vibrational mode with phonon energy of $\omega_{R2} = 768$ cm^{-1} was observed.

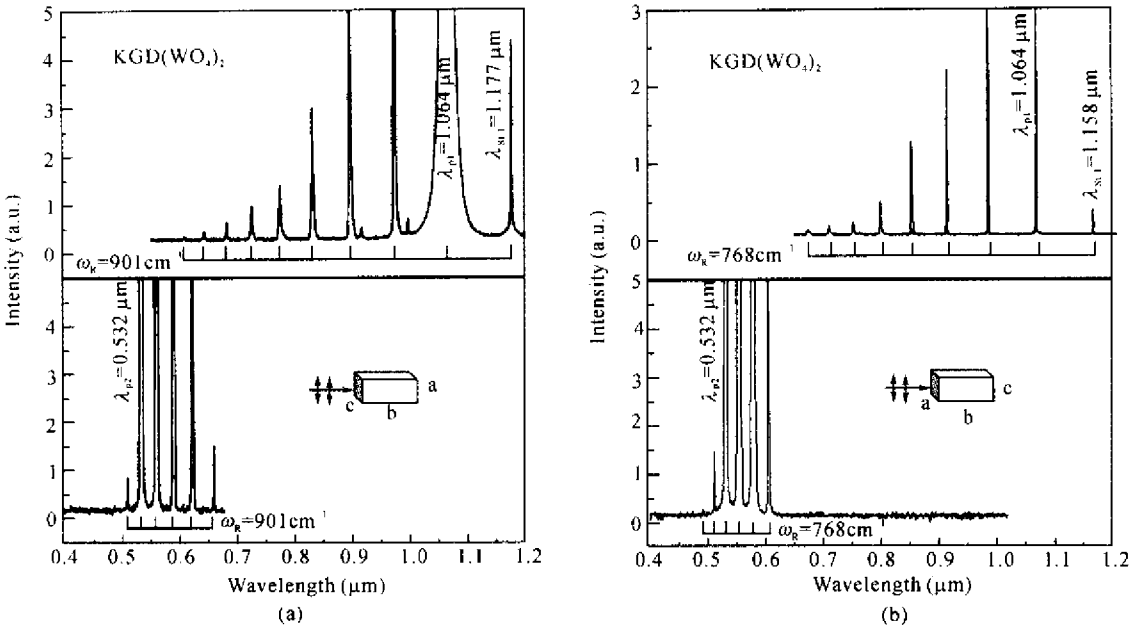

Fig.4 SRS single-pass spectra of $KGd(WO_4)_2$ crystal with excitation at 1.064 μm and 0.532 μm, generating line shifts from (a) SRS-active vibrational mode $\omega_R = 901$ cm^{-1} under excitation geometry a(bb)a and (b) SRS-active vibrational mode $\omega_R = 768$ cm^{-1} under excitation geometry c(bb)c

We investigated SRS with the fundamental frequency and second harmonic lines of a picosecond Nd: YAG laser in about 64 Raman active crystals. About 1000 SRS wavelengths from 400 to 1200 nm were observed (Table 3). In Table 4 we give an overview of wavelengths emitted by Raman-active crystals which are suitable for the creation of Raman lasers from the visible to near IR region.

Table 3 Selected Raman shifted lines for $Ba(NO_3)_2$, $KGd(WO_4)_2$ and $PbWO_4$

λ_R (nm)	Line	SRS-and RFWM-line attribution	ω_R (cm^{-1})	Crystal	Pump (nm)
473	AS_2	$\omega_{f2} + 2\omega_R$	768	$KGd(WO_4)_2$	532.07
485.5	AS_2	$\omega_{f2} + 2\omega_R$	901	$PbWO_4$	532.07
507.7	AS_1	$\omega_{f2} + \omega_R$	901	$KGd(WO_4)_2$	532.07
507.7	AS_1	$\omega_{f2} + \omega_R$	901	$PbWO_4$	532.07
511.2	AS_1	$\omega_{f2} + \omega_R$	768	$KGd(WO_4)_2$	532.07
543.3	AS_{10}	$\omega_{f1} + 10\omega_R$	901	$PbWO_4$	1064.15
554.7	S_1	$\omega_{f2} - \omega_R$	768	$KGd(WO_4)_2$	532.07
558.9	S_1	$\omega_{f2} - \omega_R$	901	$KGd(WO_4)_2$	532.07
558.9	S_1	$\omega_{f2} - \omega_R$	901	$PbWO_4$	532.07

Continued in the next page

λ_R (nm)	Line	SRS-and RFWM-line attribution	ω_R (cm^{-1})	Crystal	Pump (nm)
559	S_1	$\omega_{f2}-\omega_R$	901	$KGd(WO_4)_2$	532.07
563	S_1	$\omega_{f5}-\omega_R$	1047	$Ba(NO_3)_2$	532.07
571.2	AS_9	$\omega_{f1}+9\omega_R$	901	$PbWO_4$	1064.15
579.4	S_2	$\omega_{f2}-2\omega_R$	768	$KGd(WO_4)_2$	532.07
588.5	S_2	$\omega_{f2}-2\omega_R$	901	$KGd(WO_4)_2$	532.07
588.5	S_2	$\omega_{f2}-2\omega_R$	901	$PbWO_4$	532.07
589	S_2	$\omega_{f2}-2\omega_R$	901	$KGd(WO_4)_2$	532.07
589	SHG	$2\omega_{f1}$	901	$KGd(WO_4)_2$	1064.15
599	S_2	$\omega_{f5}-2\omega_R$	1047	$Ba(NO_3)_2$	532.07
602.2	AS_8	$\omega_{f1}+8\omega_R$	901	$KGd(WO_4)_2$	1064.15
602.2	AS_8	$\omega_{f1}+8\omega_R$	901	$PbWO_4$	1064.15
606.4	S_3	$\omega_{f2}-3\omega_R$	768	$KGd(WO_4)_2$	532.07
621.5	S_3	$\omega_{f2}-3\omega_R$	901	$KGd(WO_4)_2$	532.07
621.5	S_3	$\omega_{f2}-3\omega_R$	901	$PbWO_4$	532.07
636.8	AS_7	$\omega_{f1}+7\omega_R$	901	$KGd(WO_4)_2$	1064.15
636.8	AS_7	$\omega_{f1}+7\omega_R$	901	$PbWO_4$	1064.15
639	S_3	$\omega_{f5}-3\omega_R$	1047	$Ba(NO_3)_2$	532.07
658.3	S_4	$\omega_{f5}-4\omega_R$	901	$KGd(WO_4)_2$	532.07
675.5	AS_6	$\omega_{f1}+6\omega_R$	901	$KGd(WO_4)_2$	1064.15
675.5	AS_6	$\omega_{f1}+6\omega_R$	901	$PbWO_4$	1064.15
676.9	AS_7	$\omega_{f1}+7\omega_R$	768	$KGd(WO_4)_2$	1064.15
714	AS_6	$\omega_{f1}+6\omega_R$	768	$KGd(WO_4)_2$	1064.15
719.3	AS_5	$\omega_{f1}+5\omega_R$	901	$KGd(WO_4)_2$	1064.15
719.3	AS_5	$\omega_{f1}+5\omega_R$	901	$PbWO_4$	1064.15
736.1	AS_4	$\omega_{f1}+4\omega_R$	1047	$Ba(NO_3)_2$	1064.15
755.5	AS_5	$\omega_{f1}+5\omega_R$	768	$KGd(WO_4)_2$	1064.15
769.2	AS_4	$\omega_{f1}+4\omega_R$	901	$KGd(WO_4)_2$	1064.15
769.2	AS_4	$\omega_{f1}+4\omega_R$	901	$PbWO_4$	1064.15
788.8	S_1 from AS_4	$\omega_{f1}+4\omega_{R1}-\omega_{R2}$	$\omega_{R1}=901$; $\omega_{R2}=323$	$PbWO_4$	1064.15
797.6	AS_3	$\omega_{f1}+3\omega_R$	1047	$Ba(NO_3)_2$	1064.15
801	AS_4	$\omega_{f1}+4\omega_R$	768	$KGd(WO_4)_2$	1064.15
804.9	AS_1 from AS_3	$\omega_{f1}+3\omega_{R1}+\omega_{R2}$	$\omega_{R1}=901$; $\omega_{R2}=323$	$PbWO_4$	1064.15
826.4	AS_3	$\omega_{f1}+3\omega_R$	901	$KGd(WO_4)_2$	1064.15
826.4	AS_3	$\omega_{f1}+3\omega_R$	901	$PbWO_4$	1064.15
849.1	S_1 from AS_3	$\omega_{f1}+3\omega_{R1}+\omega_{R2}$	$\omega_{R1}=901$; $\omega_{R2}=323$	$PbWO_4$	1064.15
854.6	AS_3	$\omega_{f1}+3\omega_R$	768	$KGd(WO_4)_2$	1064.15
867.9	AS_1 from AS_2	$\omega_{f1}+2\omega_{R1}+\omega_{R2}$	$\omega_{R1}=901$; $\omega_{R2}=323$	$PbWO_4$	1064.15
870.2	AS_2	$\omega_{f1}+2\omega_R$	1047	$Ba(NO_3)_2$	1064.15
892.9	AS_2	$\omega_{f1}+2\omega_R$	901	$KGd(WO_4)_2$	1064.15
892.9	AS_2	$\omega_{f1}+2\omega_R$	901	$PbWO_4$	1064.15
914.7	AS_2	$\omega_{f1}+2\omega_R$	768	$KGd(WO_4)_2$	1064.15

Continued in the next page

λ_R (nm)	Line	SRS-and RFWM-line attribution	ω_R (cm^{-1})	Crystal	Pump (nm)
919.4	S_1 from AS_2	$\omega_{f1} + 2\omega_{R1} + \omega_{R2}$	$\omega_{R1} = 901$; $\omega_{R2} = 323$	$PbWO_4$	1064.15
941.6	AS_1 from AS_1	$\omega_{f1} + \omega_{R1} + \omega_{R2}$	$\omega_{R1} = 901$; $\omega_{R2} = 323$	$PbWO_4$	1064.15
957.5	AS_1	$\omega_{f1} + \omega_R$	1047	$Ba(NO_3)_2$	1064.15
971.1	AS_1	$\omega_{f1} + \omega_R$	901	$KGd(WO_4)_2$	1064.15
971.1	AS_1	$\omega_{f1} + \omega_R$	901	$PbWO_4$	1064.15
983.8	AS_1	$\omega_{f1} + \omega_R$	768	$KGd(WO_4)_2$	1064.15
1002.6	S_1 from AS_1	$\omega_{f1} + \omega_{R1} - \omega_{R2}$	$\omega_{R1} = 901$; $\omega_{R2} = 323$	$PbWO_4$	1064.15
1028.8	AS_1	$\omega_{f1} + \omega_R$	323	$PbWO_4$	1064.15
1102.0	S_1	$\omega_{f1} - \omega_R$	323	$PbWO_4$	1064.15
1158	S_1	$\omega_{f1} - \omega_R$	768	$KGd(WO_4)_2$	1064.15
1177	S_1	$\omega_{f1} - \omega_R$	901	$KGd(WO_4)_2$	1064.15
1177	S_1	$\omega_{f1} - \omega_R$	901	$PbWO_4$	1064.15
1197	S_1	$\omega_{f1} - \omega_R$	1047	$Ba(NO_3)_2$	1064.15
1216	S_1	$\omega_{f2} - \omega_R$	1047	$Ba(NO_3)_2$	1079[a]
1316.6	S_2	$\omega_{f1} - \omega_R$	901	$PbWO_4$	1064.15
1369	S_2	$\omega_{f1} - 2\omega_R$	1047	$Ba(NO_3)_2$	1064.15
1394	S_2	$\omega_{f2} - 2\omega_R$	1047	$Ba(NO_3)_2$	1079[a]
1529	S_1	$\omega_{f3} - \omega_R$	1047	$Ba(NO_3)_2$	1318
1556	S_1	$\omega_{f4} - \omega_R$	1047	$Ba(NO_3)_2$	1338[b]
1598	S_3	$\omega_{f1} - 3\omega_R$	1047	$Ba(NO_3)_2$	1064.15
1632	S_3	$\omega_{f2} - 3\omega_R$	1047	$Ba(NO_3)_2$	1079[a]

[a,b]: Pumped with Nd^{3+}: $YAlO_3$ laser

Table 4 List of suitable wavelengths for the creation of Raman lasers from the visible to near IR region

Wavelength (μm)	Line	Crystal
0.421	AS	$KAl(SO_4)_2 \cdot 12H_2O$
⋮	25 lines	
0.481	AS	$Ca_2Zn_2SiO_7$
0.483	AS	$Ca_2Mg_2SiO_7$
0.484	AS	$NaClO_3$
0.486	AS	$GdVO_4$
0.488	AS	$LiCaAlF_6$
⋮	400 lines	
0.821	AS	$Sc_2(MoO_4)_3$
0.822	AS	$Gd_3Ga_5O_{15}$
0.824	AS	$SrWO_4$
0.825	AS	$Bi_4Ge_3O_{12}$
0.826	AS	$KCd(WO_4)_2$
0.827	AS	$Ca(Nb_3O)_2$
0.828	AS	$Ca(NbGa)_2Ga_3O_{12}$
⋮	300 lines	
1.174	S	$CdVO_4$
1.175	S	$SrMoO^4: Nd^{3+}$
1.176	S	YVO_4
1.177	S	$KLa(MoO_4)_3$
⋮	10 lines	
1.317	S	$PbWO_4$

RAMAN LASER SETUP

By building a resonator around the Raman medium, the pump threshold was greatly reduced, the conversion efficiency was increased and better spatial quality was obtained. To obtain high energy conversion efficiency in the Raman cavity it was necessary to optimize the input beam waist diameter and interaction length. A short plano-concave cavity was chosen to achieve a small output beam size, small divergent angle, easy alignment and overall compactness. It is possinble to prepare mirrors with optimal reflectivity for the first Stokes wavelength and low reflectivity for the second-Stokes component. This increases the intensity in the first Stokes component. By varying the reflectivity of the cavity mirrors we could achieve Raman laser emission only at the first or only at the second or at the third Stokes component, independently (Fig.5).

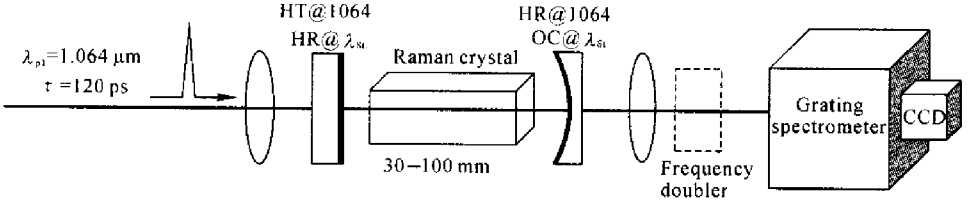

Fig.5 Experimental setup with Stokes-line amplification in a linear resonator for Raman laser with excitation wavelengths at 1.064 μm

The first Raman pulse generated in the single pass geometry was reflected to the cavity i.e. the main part of the Stokes field remained in the cavity. The pump pulse then circulated inside the resonator, amplifying the Stokes field every round trip. After the first round trip, the Stokes field had grown significantly so that the second emitted Raman pulse had more energy. Then, during further passes of the Stokes field, the pump field was considerably reduced so that the energy of the outcoming Raman pulses had decreasing trend.

RAMAN LASER RESULTS

1. Spectral emission of a $KGd(WO_4)_2$ Raman laser

The 47 mm long KGd crystal showed laser action at two different wavelengths $\lambda_{St.1} = 1.177$ μm (as shown in Fig.6a) and $\lambda_{St.1} = 1.159$ μm (as shown in Fig.6b) with phonon energies of $\omega_{R1} = 901$ cm^{-1} and $\omega_{R2} = 768$ cm^{-1}, respectively. The first-Stokes KGd Raman laser at wavelengths $\lambda_{St.1} = 1.177$ μm was generated with energy 2.1 mJ and conversion efficiency of 70%. Furthermore, the first-Stokes KGd Raman laser at wavelengths $\lambda_{St.1} = 1.159$ μm was generated with energy of 1.7 mJ and conversion efficiency 50%. The KGd Stokes emissions at $\lambda_{St.1}$

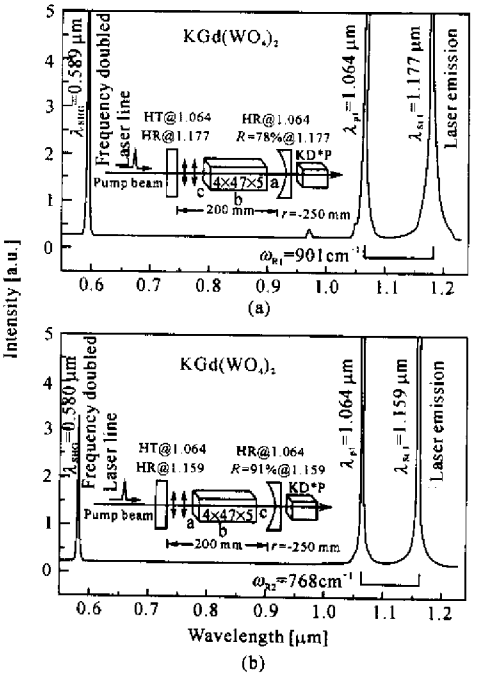

Fig.6 $KGd(WO_4)_2$ in external-cavity Raman emission: interaction with (a) 901 cm^{-1} and (b) 768 cm^{-1} vibrational mode and its second harmonic in the visible region

= 1.177 μm and $\lambda_{St.1}$ = 1.159 μm were frequency doubled with a LBO crystal at λ_{SHG} = 0.589 μm and λ_{SHG} = 0.580 μm with energies of 0.3 and 0.2 mJ, respectively. Fig.7 shows the output energy against the pump energy of the first-Stokes KGd Raman laser at (a) $\lambda_{St.1}$ = 1.159 μm and (b) $\lambda_{St.1}$ = 1.177 μm. The output energy of the Raman laser emission depends on the pump energy.

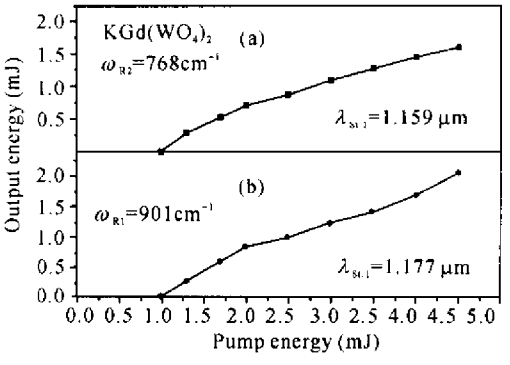

Fig.7 Dependence of the output energy on the pump energy for KGd(WO_4)$_2$ Raman emission with (a) 768 cm^{-1} and (b) 901 cm^{-1} vibrational mode interaction

Experimental measurement of the first-Stokes KGd Raman laser at $\lambda_{St.1}$ = 1.177 μm wavelength is shown in Fig.8a. The first Stokes generated an output beam with diameter $\approx$ 1.7 mm. The profile was taken with an Si-CCD array behind the output-coupler and fitted well Gaussian distribution. Fig.8b shows the time distribution of the first Stokes KGd Raman laser at $\lambda_{St.1}$ = 1.177 μm wavelength. The pulse train emitted by the resonator was measured with a photodiode and an oscilloscope. More than seven Raman pulses were emitted with a time separation of 1.3 ns corresponding to the Raman cavity round trip time. The total duration of the seven emitted Raman pulses was $\approx$8 ns.

2. First-and second-Stokes Raman laser emission from $PbWO_4$

To achieve efficient first-Stokes $PbWO_4$ Raman laser at wavelength $\lambda_{St.1}$ = 1.177 μm with high beam quality, a 200-mm plano-concave cavity was used. The output coupler had HR for the fundamental at λ_{PI} = 1.064 μm and reflectivity of 78% at the first Stokes Raman emission

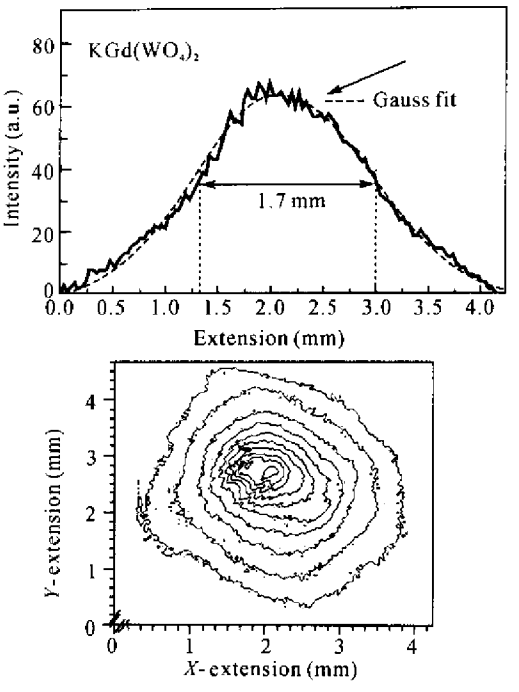

Fig.8a Beam profile of KGd(WO_4)$_2$ Raman laser

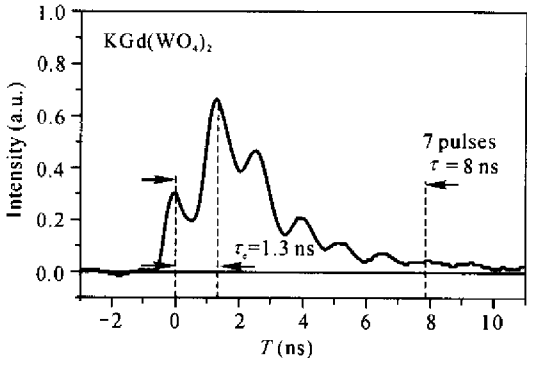

Fig.8b Temporal profile of KGd(WO_4)$_2$ Raman laser pulses

at $\lambda_{St.1}$ = 1.177 μm. First Stokes $PbWO_4$ Raman laser was generated with energy of 1 mJ, conversion efficiency of 40%, and phonon energy of ω_{RI} = 901 cm^{-1}. The Raman emission at wavelength $\lambda_{St.1}$ = 1.177 μm was frequency doubled at wavelength λ_{SHG} = 0.589 μm and energy of 0.1 mJ (see Fig.9).

Output coupler with HR for the fundamental at λ_{PI} = 1.064 μm and the first Stokes at $\lambda_{St.1}$ = 1.177 μm and with reflectivity 14% at the second-Stokes emission at $\lambda_{St.1}$ = 1.317 μm was chosen to generate second Stokes $PbWO_4$ Raman laser (Fig.10 shows the resulting spectral emis-

sion). Before the second-Stokes line could be amplified, the first-Stokes oscillation with $\lambda_{St.1} = 1.177\ \mu m$ was generated in the Raman cavity at the beginning of the laser process. It was amplified and worked as a seed for the stimulated second-Stokes scattering. After that the second-Stokes component was amplified in the Raman cavity. Then during further passes of the first-Stokes emission, the pump emission was considerably reduced and the energy of the outcoming Raman pulses had decreasing trend.

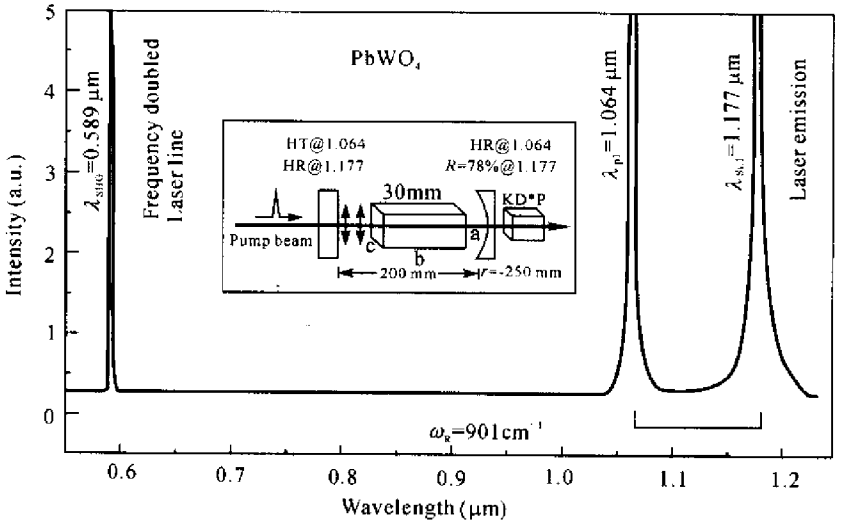

Fig.9 First-Stokes $PbWO_4$ Raman laser emission in external cavity with interacting phonon energy of 901 cm^{-1} and its second harmonic in the visible spectrum

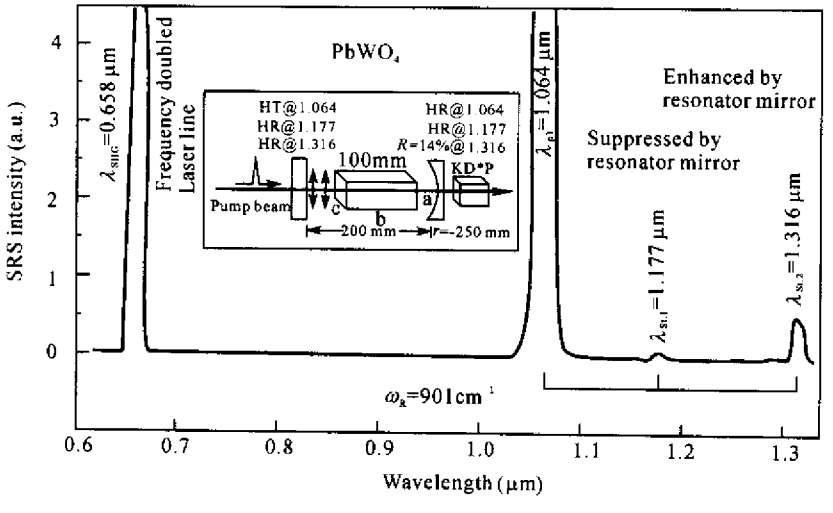

Fig.10 Second-Stokes $PbWO_4$ Raman laser emission in external cavity with interacting phonon energy of 901 cm^{-1} and its second harmonic in the visible spectrum

Fig.11 shows the second-Stokes (a) energy and (b) conversion efficiency (defined as the ratio of the output Raman laser energy to the pump energy) against the pump energy for Raman crystals with different lengths. The conversion efficiency of the second-Stokes emission depends on the Raman crystal length. Very similar behavior of Stokes generation was earlier obtained in Ba $(NO_3)_2$ Raman laser (Zverev *et al.*, 1999). For accurate measurements of the wavelength of the second-Stokes Raman laser we applied second harmonic generation SHG method by using a KD* P frequency doubler crystal. The second Stokes $PbWO_4$ Raman laser at wavelength $\lambda_{St.1} =$

1.317 μm was generated with energy of 0.85 mJ and conversion efficiency 30% and was frequency doubled at wavelength $\lambda_{SHG} = 0.658$ μm with conversion efficiency of about 10% (Fig.10).

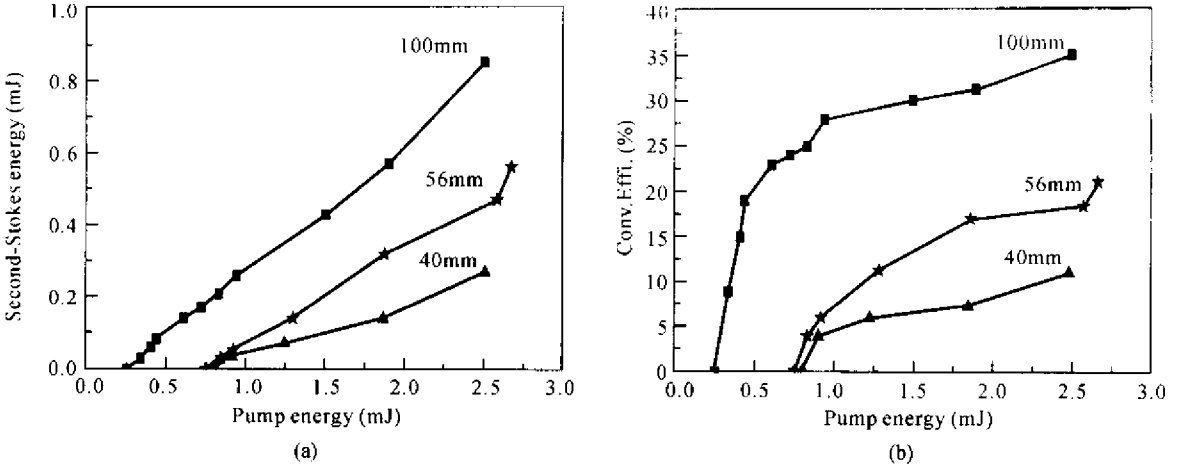

Fig.11 (a) Energy of $PbWO_4$ second-Stokes laser line versus pump energy; (b) Conversion efficiency of $PbWO_4$ second-Stokes laser line versus pump energy

The time dependency of the Raman laser emission lasting for 17.7 ns is shown in Fig.12. The cavity round-trip-time of the pump pulse was about 2 ns so that about 9 round-trips occurred before laser action stopped. The double peak at the start of laser emission is believed to be due to SRS in the two opposite directions of the crystal which caused a delay of about 1 ns.

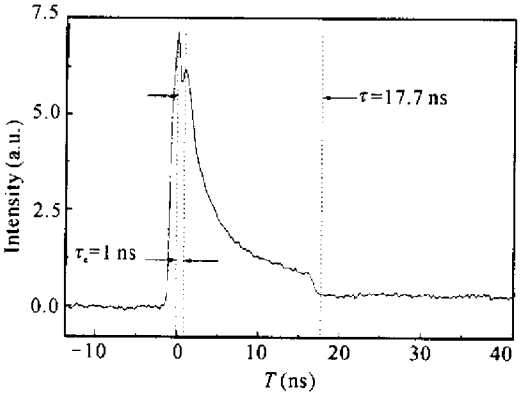

Fig. 12 Temporal emission of the $PbWO_4$ Raman laser pumped by a single pulse in an external cavity

Obtained data of our SRS experiments and results of earlier work (He *et al.*, 1997; Findeisen *et al.*, 2000; Kaminskii *et al.*, 2000) demonstrated that $PbWO_4$ crystals are attractive SRS material for obtain efficient Stokes generation in the visible and near-IR spectrum.

SUMMARY

About 64 crystals have been shown to exhibit stimulated Raman scattering on about 1000 lines covering the whole visible and near-infrared spectrum. Raman lasers increase the conversion efficiency of stimulated Raman scattering and can be constructed to emit in a single Raman line by prepared selection of the cavity mirrors. Some examples are summarized here showing that ps and ns lasers can be efficiently wavelength shifted. In the next time we will investigate anti-Stokes Raman laser that generate coherent beams with wavelengths shorter than the pump.

References

Andrjunas, K., Vistchakas, Ju., Kabelka, V., Mochalov, I.V., Pavlyuk, A.A., Petrovskii, G.T. and Syrus, V., 1985. Stimulated Raman self-conversion of Nd^{3+} laser light in double tungstenate crystals. *JETP Lett.*, **42**: 333.

Berenberg, V.A., Karpukhin, S.N. and Mochalov, I.V., 1987. Stimulated Raman scattering of nanosecond pulses in a $KGd(WO_4)_2$ crystal. *Sov. J. Quant. Electron*, **14**: 1849.

Eremenko, A.S., Karpukhin, S.N. and Stepanov, A.I., 1980. Stimulated Raman scattering of the second harmonic of a neodymium laser in nitrate crystals. *Sov. J. Quantum Electron*, **10**: 113.

Findeisen, J., Eichler, H.J. and Kaminskii, A.A., 1999. Efficient picosecond $PbWO_4$ and two-wavelength $KGd(WO_4)_2$ Raman lasers in the IR and visible. *IEEE J. Quant. Electron*, **35**:173.

Findeisen, J., Eichler, H.J., Peuser, P., Kaminskii, A. A. and Hulliger, J., 2000. Diode-pumped $Ba(NO_3)_2$ and $NaBrO_3$ Raman lasers. *Appl. Phys. B*, **70**:159.

Gad, G.M.A., Eichler, H.J. and Kaminskii, A.A., 2003. Highly efficient 1.3-μm second Stokes $PbWO_4$ Raman lasers. *Opt. Lett.*, **28**:426.

Grabtchikov, A.S., Kuzmin, A.N., Lisinetskii, V.A., Ryabtsev, G.I., Orlovich, V.A. and Demidovich, A. A., 2000. Stimulated Raman scattering in Nd: KGW laser with diode pumping. *J. Alloys and Compounds*, **300**:300.

Grabtchikov, A.S., Kuzmin, A.N, Lisinetskii, V.A., Orlovich, V.A., Demidovich, A.A., Yumashev, K. V., Kuleshov, N.V., Eichler, H.J. and Danailov, M.B., 2001. Passively Q-switched 1.35 μm diode pumped Nd: KGW laser with V: YAG saturable absorber. *Optical Materials*, **16**:349.

He, C. and Chyba, T.H., 1997. Solid-state barium nitrate Raman laser in the visible region. *Opt. Commun.*, **135**: 273.

Kaminskii, A.A., Ustimenko, N.S., Gulin, A.V., Bagaev, S.N. and Pavlyuk, A.A., 1998. Raman parametric interactions in $KGd(WO_4)_2$ and $KGd(WO_4)_2$: Nd^{3+} monoclinic crystals: picosecond multicomponent Stokes and anti-Stokes emission and nanosecond stimulated Raman scattering self-conversion into eye-safe 1.5-μm wavelength range. *Dokal. Russian Akad. Nauk*, **359**:179.

Kaminskii, A.A., Eichler, H.J., Ueda, K., Klassen, N. V., Redkin, B.S., Li, L.E., Findeisen, J., Jaque, D., Garcia-Sole, J., Fernandez, J. and Balda, R., 1999. Properties of Nd^{3+}-doped and undoped tetragonal $PbWO_4$, $NaY(WO_4)_2$, $CaWO_4$, and undoped monoclinic $ZnWO_4$ and $CdWO_4$ as laser-active and stimulated Raman scattering-active crystals. *Appl. Opt.*, **38**:4533.

Kaminskii, A.A., McCray, C.L., Lee, H.R., Lee, S. W., Temple, D.A., Chyba, T.H., Marsh, W.D., Barnes, J.C., Annanenkov, A.N., Legun, V.D., Eichler, H.J., Cad, G.M.A. and Ueda, K., 2000. High efficiency nanosecond Raman lasers based on tetragonal $PbWO_4$ crystals. *Opt. Comm.*, **183**:277.

Karpukhin, S.N. and Stepanov, A.I., 1986. Generation of radiation in a resonator under conditions of stimulated Raman scattering in $Ba(NO_3)_2$, $NaNO_3$ and $CaCO_3$ crystals. *Sov. J. Quantum Electron.*, **16**:1027.

Orlovich, V.A., Kiefer, W., Apanasevich, P.A., Buj, A.A., Grabtchikov, A.S., Kachinsky, A.V., Ermolenkov, V.V. and Kruglik, S.G., 2000. All-solid-state stimulated Raman scattering-based source of pulsed radiation tunable in 345 – 625 and 690 – 1250 nm ranges for spectroscopic applications. *J. Raman Spectr.*, **31**:851.

Zverev, P.G., Basiev, T.T. and Prokhorov, A.M., 1999. Stimulated Raman scattering of laser radiation in Raman crystals. *Opt. Materials.*, **11**:335.